






Control Techniques Applied to Two Degrees of Freedom Planar Robotic Arm

J G Maradey-Lazaro¹^a, A D Rincon-Quintero^{2,3}^b, Kevin Sebastián Caceres-Mojica¹^c, C L Sandoval-Rodriguez^{2,3}^d and O Lengerke¹^e

¹Universidad Autónoma de Bucaramanga UNAB, Bucaramanga Santander 680003, Colombia

²Unidades Tecnológicas de Santander UTS, Bucaramanga Santander 680005, Colombia

³University of the Basque Country UPV/EHU, Bizkaia 48013, Spain

Keywords: Control design, control Techniques applied, degrees of freedom, mechatronics systems, robotic arm.

Abstract: The automation of production processes using robotic manipulators seems to be one of the most advanced technological areas in the last decade, as it provides the possibility of manipulating objects through a versatile and automatic configuration of manufacturing systems. This type of robot has several uses which can make the work much easier and safer, offering precision and quality to the development of designated activities in the world of automation. To obtain this goal, effective control techniques offer a practical alternative to analyze the behavior of the mechatronics systems considering the natural dynamic of the system and to select the best for each application, respectively. This article aims to design a robot with two degrees of freedom for which the dynamic model was obtained, in addition to performing the control design that ensures the stability of the system, in which the position is measured to obtain the error difference between the desired value and the actual value.

1 INTRODUCTION


In recent years, it is very common to find in the automation and control industry, systems or mechanisms that are useful for performing tasks or activities involving planar-type robots. An indicator of the effectiveness of robotic in improving manufacturing processes is the efforts made in automatization, industrial and robotic areas (Kouritem et al., 2022)(Rincon-Quintero, Sandoval-Rodríguez, et al., 2022).


Considering competitiveness as a key factor to remain in the market, industrial companies are working to establish a balance between human labor and the use of robots, in addition to tools for interaction and collaboration that bring efficiency to the work being faster, more precise,


flexible, in a way that significantly reduces the cost of production (Xu et al., 2022)(Mendoza-Calderón et al., 2022).


While it is true, it is not possible to modify 100% of the work performed by a human being, the specific robotic arm can be extremely useful for the tasks of assembly and movement of parts or raw material.


It is important to mention that the position and orientation of the final effector of the robotic arm must be considered for the robotic arm to perform a specific task, which means that a previous configuration must be taken concerning an initial reference frame. In addition, a speed and acceleration analysis are necessary to perform uniform motion control in the robotic system (Kayastha et al., 2022)(Rincon-Quintero,

^a  <https://orcid.org/0000-0003-2319-1965>

^b  <https://orcid.org/0000-0002-4479-5613>

^c  <https://orcid.org/0000-0002-7863-915X>

^d  <https://orcid.org/0000-0001-8584-0137>

^e  <https://orcid.org/0000-0001-9360-7319>

Del Portillo-Valdés, Meneses-Jácome, Ascanio-Villabona, et al., 2021).

Based on this information, a series of advanced control strategies are proposed, to adapt the most efficient and optimal technique, thus obtaining a better version of a two-degree planar robotic arm of freedom. Therefore, three control strategies have been studied in the next sections: PID, LQR (i.e Linear-Quadratic regulator) control and observer for pole location, and LQG (i.e Linear—Quadratic-Gaussian) control and filter of Kalman using values such as IAE (i.e., Integral absolute Error), ITAE (i.e., Integral Time Absolute Error), ISE (i.e., Integral Square Error), and ITSE (i.e., Integral Time Square Error).

2 MATHEMATICAL MODEL

This modeling presents the description of the dynamics of a two-degrees of freedom planar robot, which exposes its main characteristics in Figure 1 (Ni et al., 2022).

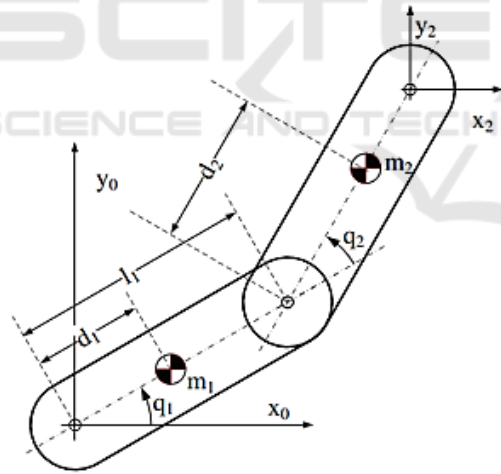


Figure 1 : The two-degree flat robotic arm of freedom (Ni et al., 2022).

Below are the coordinates and speeds of the centers of mass of element 1. It is important to mention that C1, S1, C12 and S12 correspond to Cos(q1), Sin(q1), Cos(q1+q2) and Sin(q1+q2) respectively.

$$x_1 = d_1 C_1 \tag{1}$$

$$\dot{x}_1 = -d_1 S_1 \dot{q}_1 \tag{2}$$

$$y_1 = d_1 S_1 \tag{3}$$

$$\dot{y}_1 = d_1 C_1 \dot{q}_1 \tag{4}$$

And using the above equations you can set the following:

$$v_1^2 = \dot{x}_1^2 + \dot{y}_1^2 = d_1^2 \dot{q}_1^2 \tag{5}$$

Below are the coordinates and speeds of the mass centers of element 2.

$$x_2 = l_1 C_1 + d_2 C_{12} \tag{6}$$

$$\dot{x}_1 = -(l_1 S_1 + d_2 S_{12}) \dot{q}_1 - d_2 S_{12} \dot{q}_2 \tag{7}$$

$$y_2 = l_1 S_1 + d_2 S_{12} \tag{8}$$

$$\dot{y}_1 = (l_1 C_1 + d_2 C_{12}) \dot{q}_1 + d_2 C_{12} \dot{q}_2 \tag{9}$$

And using the above equations you can set the following:

$$v_2^2 = \dot{x}_2^2 + \dot{y}_2^2 = (l_1^2 + d_2^2 + 2l_1 d_2 C_2) \dot{q}_1^2 + d_2^2 \dot{q}_2^2 + 2d_2(l_1 C_2 + d_2) \dot{q}_1 \dot{q}_2 \tag{10}$$

Below are the equations corresponding to the kinetic energy and potential energy of the system respectively.

$$E_c = \frac{1}{2}(m_1 v_1^2 + m_2 v_2^2) = \frac{1}{2}[m_1 d_1^2 + m_2(l_1^2 + d_2^2 + 2l_1 d_2 C_2)] \dot{q}_1^2 \tag{11}$$

$$E_p = g(m_1 h_1 + m_2 h_2) = g(m_1 y_1 + m_2 y_2) = g(m_1 d_1 S_1 + m_2 l_1 S_1 + m_2 d_2 S_{12}) \tag{12}$$

Lagrangian is now applied to the above equations by getting the following:

$$L = E_c - E_p = \frac{1}{2}[m_1 d_1^2 + m_2(l_1^2 + d_2^2 + 2l_1 d_2 C_2)] \dot{q}_1^2 + \frac{1}{2}[m_2 2d_2(l_1 C_2 + d_2)] \dot{q}_1 \dot{q}_2 - g(m_1 d_1 S_1 + m_2 l_1 S_1 + m_2 d_2 S_{12}) \tag{13}$$

Finally, the final equations corresponding to:

$$T1 = [m_1 d_1^2 + m_2(l_1^2 + d_2^2 + 2l_1 d_2 \cos(q_2))] \dot{q}_1^2 + [m_2 d_2(l_1 \cos(q_2) + d_2)] \dot{q}_2 - [2m_2 l_1 d_2 \sin(q_2)] \dot{q}_1 \dot{q}_2 + g[(m_1 d_1 + m_2 l_1) \cos(q_1) + m_2 d_2 \cos(q_1 + q_2)] \tag{14}$$

$$T2 = [m_2 d_2 (l_1 \cos(q_2) + d_2)] \ddot{q}_1 + [m_2 d_2^2] \ddot{q}_2 - [m_2 d_2 l_1 \sin(q_2)] \dot{q}_1 \dot{q}_2 + [m_2 d_2 l_1 \sin(q_2)] \dot{q}_1^2 + [m_2 d_2 l_1 \sin(q_2)] \dot{q}_1 \dot{q}_2 + g m_2 d_2 \cos(q_1 + q_2) \quad (15)$$

2.1 State Space System Model

Based on the above equations it is possible to formulate the two degrees of freedom planar arm system in state space, to apply a complete and robust multivariate control to the model (Rincon-Quintero, Portillo-Valdés, et al., 2021). Table 1 shows the System States of 2 DOF Planar Robotic Arm and Table 2 report the inputs to the model. Similarly, in the Table 3 the numerical parameters taken to run the model are shown.

$$\dot{X} = A * X + B * u \quad (16)$$

$$Y = C * X + D * u \quad (17)$$

Table 1 : System States.

2DOF Planar Robotic Arm States		
States	Nomenclature	Variable
Link position 1	$x(t)$	q_1
Link position 2	$x_2(t)$	\dot{q}_1
Link speed 1	$x_3(t)$	q_2
Link speed 2	$x_4(t)$	\dot{q}_2

Table 2. System Inputs

2DOF Planar Robotic Arm System Inputs		
Inputs	Nomenclature	Variable
Link Torque 1	$u_1(t)$	T_1
Link Torque 2	$u_2(t)$	T_2

In this way, the equations of the system in state space are the following:

$$X = \begin{bmatrix} q_1 \\ \dot{q}_1 \\ q_2 \\ \dot{q}_2 \end{bmatrix}; \quad A = \begin{bmatrix} 0 & 1 & 0 & 0 \\ 0 & 0 & 0 & 0 \\ 0 & 0 & 0 & 1 \\ 0 & 0 & 0 & 0 \end{bmatrix}; \quad (18)$$

$$B = \begin{bmatrix} 0 & 0 \\ 1 & -(d_2 + l_1) \\ \frac{d_1^2 m_1}{d_1^2 d_2 m_1} & \frac{-(d_2 + l_1)}{d_1^2 d_2 m_1} \\ 0 & 0 \\ -\frac{(d_2 + l_1)}{d_1^2 d_2 m_1} & \frac{d_1^2 m_1 + m_2 (d_1^2 + 2d_2 l_1 + l_1^2)}{d_1^2 d_2^2 m_1 m_2} \end{bmatrix}$$

$$C = \begin{bmatrix} 1 & 0 & 0 & 0 \\ 0 & 0 & 1 & 0 \end{bmatrix}; \quad D = \begin{bmatrix} 0 & 0 \\ 0 & 0 \end{bmatrix} \quad (19)$$

Table 3 : Parameters

2DOF Planar Robotic Arm Parameters		
Parameters	Value	Unit
Link mass 1	0.345	[Kg]
Link mass 2	0.106	[Kg]
Distance from link 1 to the center of mass	0.25	[m]
Distance from link 2 to the center of mass	0.11	[m]
Gravity constant	9.81	$\left[\frac{m}{s^2}\right]$
Link length 1	0.3	[m]

Subsequently, we proceed to compare the linear system of the mathematical model with the nonlinear system to establish a path that allows the multivariate control mentioned above.

Figure 2 shows the basic system states corresponding to the position of link 1 and link 2 of the two degrees of freedom planar robotic arm. From there it can be inferred that the position of link 1 has similarity in both systems (linear and nonlinear) up to approximately 0.1 degrees and that the position of link 2 to point 0.12 degrees. This allows us to conclude that the proposed linear system behaves sufficiently like the nonlinear system to apply multivariate control to the model in question.

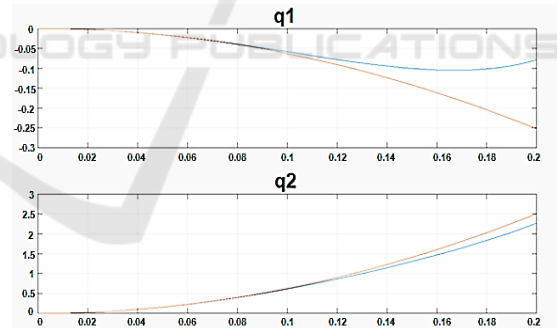


Figure 2 : Linear model and non-linear model of the system.

2.2 Control Technique PID

As a first step, a PID control technique is applied where it is possible to analyze the variables of inputs or variables to be controlled (Satya Durga Manohar Sahu et al., 2022)(Rincon-Quintero, Del Portillo-Valdés, Meneses-Jácome, Sandoval-Rodríguez, et al., 2021). In this case the torques of links 1 and 2 of the planar robotic arm of two degrees of freedom. As can be seen in Figure 3 for the first torque you have a controller that stabilizes the system in 0.839 seconds, with a lifting time of 0.463 seconds and without any

overpasses. Despite not being a very advanced control technique the results that were obtained with this first controller were very satisfactory.

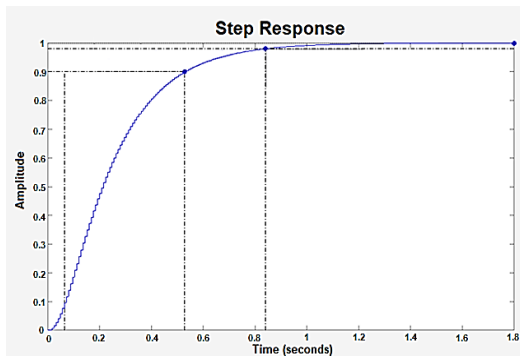


Figure 3 : Torque one closed-loop response with PID.

As a second measure, a PID-type controller is also designed for link 2 torque of the planar robotic arm. Through Figure 4 it can be observed that this torque was controlled in approximately 0.792 seconds with a lifting time of 0.443 seconds and without any overpasses. These data obtained allow analysis that although both controllers were designed separately.

They were of a PID nature, at the time of unifying them behave according to the results observed in the graphs, because they have very similar parameters, such as the establishment and lifting times of the system.

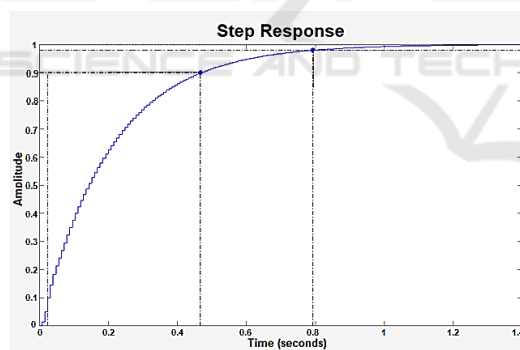


Figure 4 : Torque two closed-loop response with PID.

2.3 LQR Control Technique and Observer by Pole Location

This first advanced control technique called LQR is accompanied by an observer by pole location, this one is commonly used to estimate system states (Misra et al., 2020)(Rincon-Quintero, Del Portillo-Valdés, et al., 2022). It is important to mention that this controller allows to perform multivariate analysis, that is, to the differential of the PID control technique, this controller allows to influence both variables over time.

In Figure 5 can be observed for the first variable, i.e., link 1 torque, a signal set time of 0.806 seconds, and a lift time of 0.289 seconds. For link 2 torque, an establishment time of 0.802 seconds and a lifting time of 0.291 seconds can be seen. In addition, it is possible to claim that both variables to be controlled showed an overpass of 4.21% and 3.97%. The data obtained from both signals were very similar.

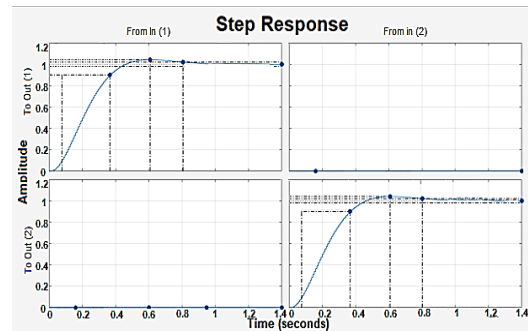


Figure 5 : The closed-loop system with LQR and pole location observer.

Based on Figure 6 you can observe the control actions of the variables affected by the control carried out above. In any case, no signal presents behavior that can negatively influence the behavior of the controlled system.

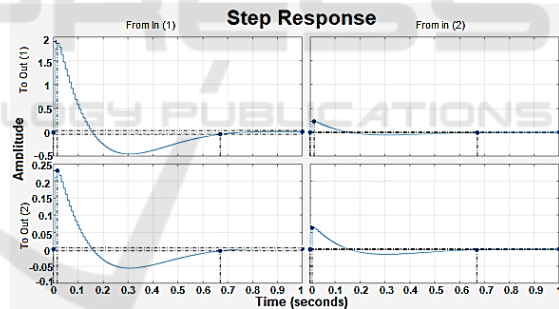


Figure 6 : Control action of the closed-loop system with LQR and observer by pole location.

2.4 Control Technique with Kalman Filter

Better known as an LQG control technique, this controller allows the union of optimal LQR control with a Kalman filter (Narayan et al., 2020)(Rybus et al., 2022). The Kalman filter is a set of mathematical equations that provides an efficient computational (recursive) solution of the least-squares method.

The filter is very powerful in several aspects: it supports estimations of past, present, and even future states, and it can do so even when the precise nature of the modeled system is unknown (Sanchez et al., 2022). This tool is useful for identifying the non-

measurable state of a linear system, in this case, the two degrees of freedom planar robotic arm. Figure 7 illustrates the closed-loop system of the model with the controlled variables, i.e., the torques of the links.

The first torque shows control with a set time of 0.812 seconds and a lifting time of 0.292 seconds. Similarly, an overpass of 4.25% can be differentiated. For link 2 it is observed that at 0.812 seconds torque 2 manages to stabilize, previously having a lifting time of 0.294 seconds and an overpass of 4.21%.

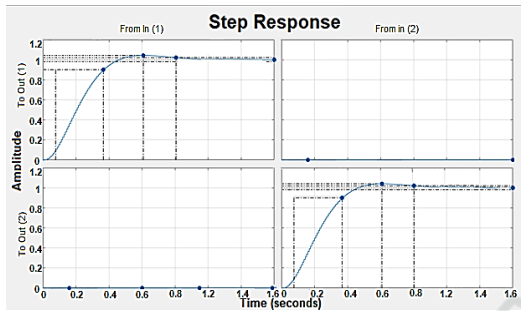


Figure 7 : The closed-loop system with LQG.

As in the previous section, Figure 8 shows the control action of each of the variables caused by the controls applied using the LQG technique. However, these signals do not affect either the working range or the behavior of the controller.

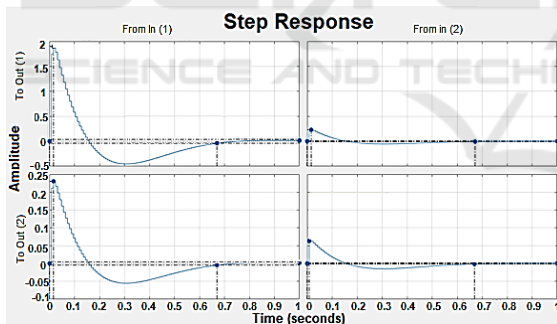


Figure 8 : Control action of the closed-loop system with LQG.

“Two-degree-of-freedom (2DOF) PID controller” is a 2DOF controller whose serial compensator is a PID element and whose feedforward compensator is a PD element (Abhishek & Kumar Dalla, 2022).

Through Figure 9 you can see a slight overpass in both variables to be controlled of 0.608%, an establishment time of 0.812 seconds, and a lifting time of 0.291 and 0.292 seconds. The great advantage of unifying these techniques is that the behavior of the variables to be controlled against a control action is almost the same.

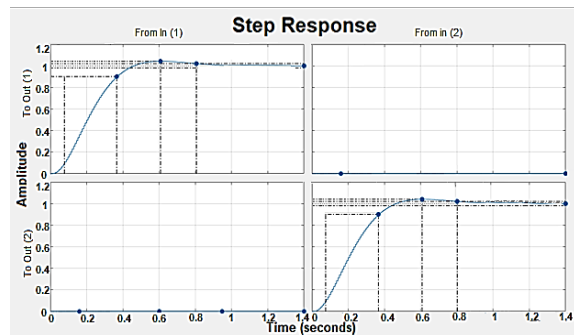


Figure 9 : The closed-loop system with two degrees of freedom control.

As shows in Figure 10, for the control action caused in the system, it possible to note the influence all variables of the model, however, in two of them the negative overstep is greater and this is mainly due to the robust and forced nature of the controller over the variables in question.

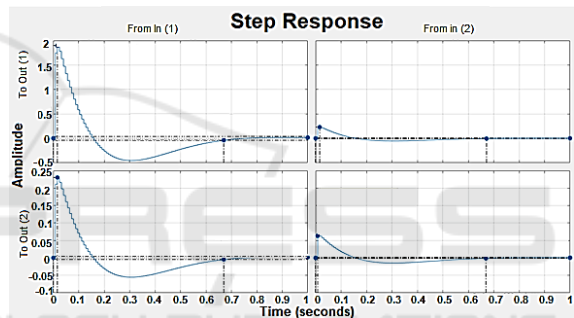


Figure 10 : Control action with two degrees of freedom control.

2.5 DOF Control Technique

For the latest applied control technique, we then have unified control of an LQR along with a Kalman filter under the 1 degree of freedom mode. The 1 DOF control technique suffers from the limitation that there exists a compromise between response and loop goal performances (Fortunato et al., 2022). It can be seen in Figure 11 that the behavior, in this case, is not the best due to a considerable overfits of 69.3% in torque 1 and another even larger overstep of 92.6% in the torque of link 2.

As for the establishment times in both cases, it was 0.716 and 0.403 seconds. And the rise time was 0.0607 and 0.0184 seconds. While it is true the times in which both torques stabilize are very good, however, the oversteps negatively affect the behavior of the signals in question.

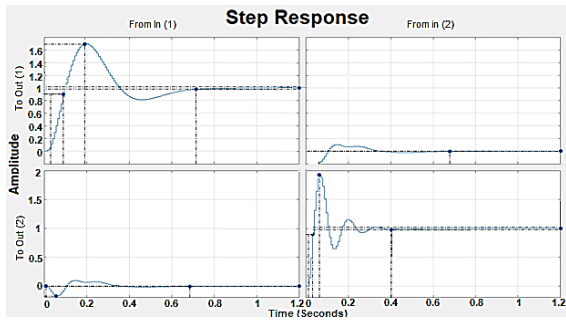


Figure 11 : Closed-loop system with one degree of freedom control.

And finally, you can see a behavior very similar to the control signal in the control action of each of the variables in Figure 12.

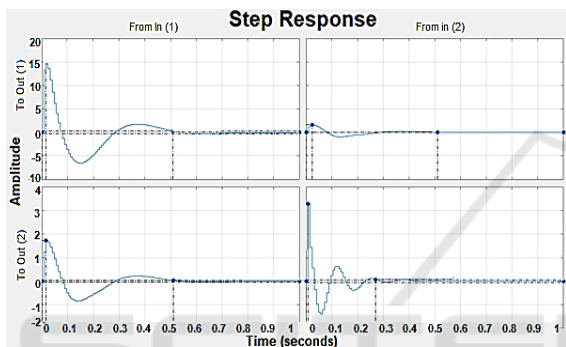


Figure 12 : Control action with control of a degree of freedom.

3 RESULTS AND CONCLUSIONS

For better compression of the digital control techniques applied above, this section shows the system behavior under the applied control technique, given a range of operations and several set points. Similarly, the nonlinear model of the system is shown in the same graph to have a closer perception of what these control strategies applied to the robot would be.

In the first comparison plot corresponding to Figure 13, it can observe the variables to be controlled, i.e., the torques of the robot links, under the PID control technique. For ranges farther from zero, you can see that the nonlinear model is not able to reach its set point, and when the set point of one variable changes, the control signal of the other variable is affected as it is a unified multivariate control. It is important to mention that the operating range for this control technique ranges from $[-\frac{\pi}{32}]$ until $[\frac{\pi}{32}]$.

In this second comparison plot (i.e Figure 14) corresponding to the LQR control technique and the observer by pole location you can see that always the variable in the process reaches its set point, however,

the same phenomenon described in the graph above occurs, where the control signal in one variable is affected when the set point of the other variable changes, this is due to the nature of the controller. The operating range for this case is from $[-\frac{\pi}{2}]$ to $[\frac{\pi}{2}]$.

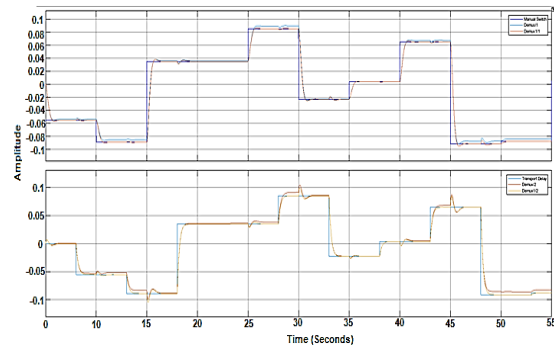


Figure 13 : Comparison of the non-linear model with PID control.

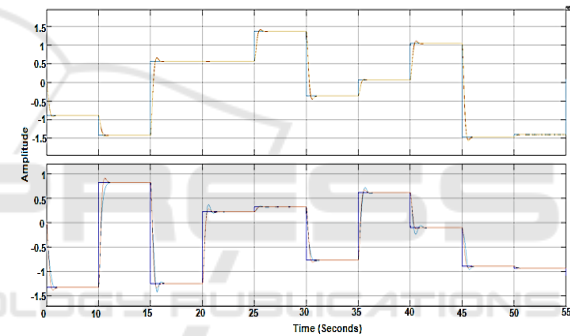


Figure 14 : Comparison of the non-linear model with LQR control and observer by pole location.

Figure 15 corresponds to the LQG control technique, where you can see that always the variable in process reaches its set point without problem, there is a minimum overshoots, and the operating range is from $[-\frac{\pi}{2}]$ to $[\frac{\pi}{2}]$. Behavior is very similar to the previous case.

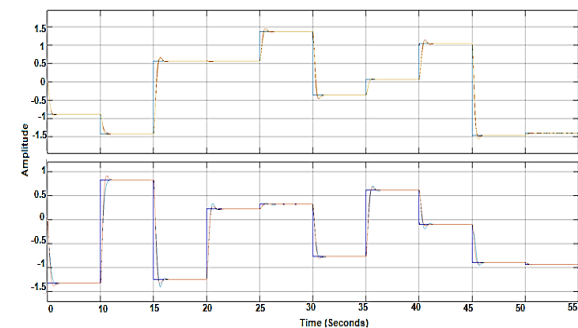


Figure 15 : Comparison of the non-linear model with LQG control.

Also, Figure 16 corresponds to the two-degree unified control technique of freedom in which optimal behavior can be observed in which the variable always reaches its stability. The operating range is from, $[-\frac{\pi}{6}]$ to $[\frac{\pi}{6}]$.

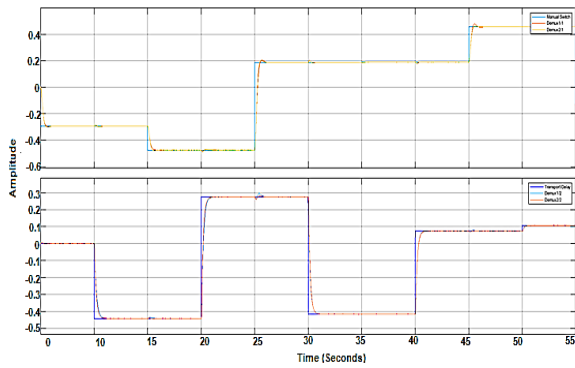


Figure 16 : Comparison of the non-linear model with 2DOF control

Finally, In Figure 17 the graph corresponding to the unified control technique is shown using the 1 degree of freedom mode. Without a doubt, the variable in the process does not have the best behavior, due to the high overpasses, however, if the point of stability is reached in both variables to be controlled.

The operating range is from, $[-\frac{\pi}{2}]$ to $[\frac{\pi}{2}]$.

For the quantitative evaluation, the error is determined from the IAE, ITAE, ISE, and ITSE values is shown in Table 4 as a summary. This, calculating the difference between the feedback signal and the operating point values, which represent the error signal, obtained from the following equations (Rahul et al., 2019).

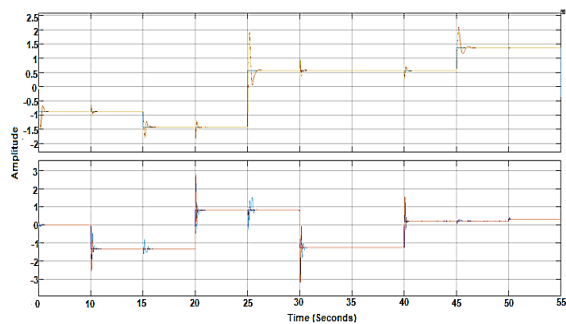


Figure 17 :Comparison of the non-linear model with the control of a degree of freedom.

$$ISE = \int_0^T e(t)dt \quad (20)$$

$$IAE = \int_0^T [e(t)]^2 dt \quad (21)$$

$$ITAE = \int_0^T t[e(t)]dt \quad (22)$$

$$ITSE = \int_0^T t[e(t)]^2 dt \quad (23)$$

Table 4 : Error Rates of the Controls applied to the System.

Error rates of the controllers applied				
Control technique	IAE	ITAE	ISE	ITSE
Control PID	0.2	6.7	0.0	0.3
	0.3	6.7	0.0	0.2
LQR control and observer por pole location	0.3	0.0	0.3	0.0
	0.4	0.1	0.3	0.0
LQR control and filter de kalman	0.3	0.0	0.3	0.0
	0.4	0.1	0.3	0.0
Control de 2DOF	0.4	0.2	0.3	0.0
	0.2	1.4	0.2	1.3
Control de 1DOF	0.5	0.3	0.4	0.3
	0.2	1.3	0.2	1.2

To make a deeper analysis in terms of the comparison of all the control techniques applied in this research article, a series of performance indices were implemented for each variable to be controlled (torque one and torque two).

The first error rate corresponds to the integral of the absolute value of the IAE error. This index usually gives longer set-up times and higher oversteps, so it is considered one of the most sensitive. The second index used is the integral of time multiplied by the absolute value of the ITAE error. In this error, the transient responses that are obtained usually have small oversteps and well-cushioned oscillations. The ISE error square integral penalizes large errors and discriminates between over-caused and sub-wet responses.

Finally, the ITSE error rate corresponding to the integral time multiplied by the error square was obtained. This is characterized mainly by giving little importance to initial errors, however, if it influences the errors present after a few seconds of the start of the system entry.

Based on the comparison of the control techniques implemented in this article, the graphs provided, and the ranges of action, it is decided that the best controllers implemented are the LQG and LQR with pole location observer, since they have a wide range of action from.

$[-\frac{\pi}{2}]$ to $[\frac{\pi}{2}]$, their error rates are minimal, their transient responses have short settling times (0.8 seconds) and very minimal overruns (4.2%).

Once again, the usefulness of these advanced control techniques for this type of robotic system, which are used with high frequency in the process

automation industry worldwide, is proven. Due to their widespread use and the diversity of models and systems, it is necessary to carry out this type of research to create solid bases for the progressive development of assisted manufacturing.

ACKNOWLEDGEMENTS

This work is supported by the research management of the Universidad Autónoma de Bucaramanga, where the research project has a grant to supports Bachelor's students in mechatronics engineering.

REFERENCES

- Abhishek, K., & Kumar Dalla, V. (2022). Formulation of kinematics and gait locomotion for Hyper-Redundant robot. *Materials Today: Proceedings*, *56*, 976–979. <https://doi.org/10.1016/j.matpr.2022.03.110>
- Fortunato, G. M., Bonatti, A. F., Batoni, E., Macaluso, R., Vozzi, G., & De Maria, C. (2022). Motion compensation system for robotic based in situ bioprinting to balance patient physiological movements. *Bioprinting*, *28*(October), e00248. <https://doi.org/10.1016/j.bprint.2022.e00248>
- Kayastha, S., Katupitiya, J., Pearce, G., & Rao, A. (2022). Comparative study of post-impact motion control of a flexible arm space robot. *European Journal of Control*, *xxxx*, 100738. <https://doi.org/10.1016/j.ejcon.2022.100738>
- Kouritem, S. A., Abouheaf, M. I., Nahas, N., & Hassan, M. (2022). A multi-objective optimization design of industrial robot arms. *Alexandria Engineering Journal*, *61*(12), 12847–12867. <https://doi.org/10.1016/j.aej.2022.06.052>
- Mendoza-Calderón, K. D., Jaimés, J. A. M., Maradey-Lazaro, J. G., Rincón-Quintero, A. D., & Cardenas-Arias, C. G. (2022). Design of an Automatic Palletizer. *Journal of Physics: Conference Series*, *2224*(1), 0–15. <https://doi.org/10.1088/1742-6596/2224/1/012095>
- Misra, A., Sharma, A., Singh, G., Kumar, A., & Rastogi, V. (2020). Design and Development of a Low-Cost CNC Alternative SCARA Robotic Arm. *Procedia Computer Science*, *171*(2019), 2459–2468. <https://doi.org/10.1016/j.procs.2020.04.266>
- Narayan, J., Mishra, S., Jaiswal, G., & Dwivedy, S. K. (2020). Novel design and kinematic analysis of a 5-DOFs robotic arm with three-fingered gripper for physical therapy. *Materials Today: Proceedings*, *28*, 2121–2132. <https://doi.org/10.1016/j.matpr.2020.04.017>
- Ni, S., Chen, W., Ju, H., & Chen, T. (2022). Coordinated trajectory planning of a dual-arm space robot with multiple avoidance constraints. *Acta Astronautica*, *195*(December 2021), 379–391. <https://doi.org/10.1016/j.actaastro.2022.03.024>
- Rahul, K., Raheman, H., & Paradkar, V. (2019). Design and development of a 5R 2DOF parallel robot arm for handling paper pot seedlings in a vegetable transplanter. *Computers and Electronics in Agriculture*, *166*(February), 105014. <https://doi.org/10.1016/j.compag.2019.105014>
- Rincon-Quintero, A. D., Del Portillo-Valdés, L. A., Meneses-Jácome, A., Ascanio-Villabona, J. G., Tarazona-Romero, B. E., & Durán-Sarmiento, M. A. (2021). *Performance Evaluation and Effectiveness of a Solar-Biomass Hybrid Dryer for Drying Homogeneous of Cocoa Beans Using LabView Software and Arduino Hardware BT - Recent Advances in Electrical Engineering, Electronics and Energy* (M. Botto Tobar, H. Cruz, & A. Díaz Cadena (eds.); pp. 238–252). Springer International Publishing.
- Rincon-Quintero, A. D., Del Portillo-Valdés, L. A., Meneses-Jácome, A., Sandoval-Rodríguez, C. L., Rondón-Romero, W. L., & Ascanio-Villabona, J. G. (2021). *Trends in Technological Advances in Food Dehydration, Identifying the Potential Extrapolated to Cocoa Drying: A Bibliometric Study BT - Recent Advances in Electrical Engineering, Electronics and Energy* (M. Botto Tobar, H. Cruz, & A. Díaz Cadena (eds.); pp. 167–180). Springer International Publishing.
- Rincon-Quintero, A. D., Del Portillo-Valdés, L. A., Zanabria-Ortigoza, N. D., Sandoval-Rodríguez, C. L., Maradey-Lázaro, J. G., & Castillo-León, N. Y. (2022). Exergy analysis and development of flat plate solar collectors: A Review. *IOP Conference Series: Materials Science and Engineering*, *1253*(1), 012009. <https://doi.org/10.1088/1757-899x/1253/1/012009>
- Rincon-Quintero, A. D., Portillo-Valdés, L. A. Del, Cárdenas-Arias, C. G., Tarazona-Romero, B. E., Rondón-Romero, W. L., & Durán-Sarmiento, M. A. (2021). A bibliometric analysis of the uses of the cocoa pod shell. *IOP Conference Series: Materials Science and Engineering*, *1154*(1), 012032. <https://doi.org/10.1088/1757-899x/1154/1/012032>
- Rincon-Quintero, A. D., Sandoval-Rodríguez, C. L., Lengerke-Perez, O., Rueda-Osma, M. F., & Mateus-Ariza, J. A. (2022). *Evaluation and Control of Psychrometric Variables Present in an Automated Greenhouse for the Production of Organic Tomato BT - Recent Advances in Electrical Engineering, Electronics and Energy* (M. Botto-Tobar, H. Cruz, & A. Díaz Cadena (eds.); pp. 165–180). Springer International Publishing.
- Rybus, T., Wojtunik, M., & Basmadji, F. L. (2022). Optimal collision-free path planning of a free-floating space robot using spline-based trajectories. *Acta Astronautica*, *190*(June 2021), 395–408. <https://doi.org/10.1016/j.actaastro.2021.10.012>
- Sanchez, M., Cruz-Ortiz, D., Ballesteros, M., Salgado, I., &

- Chairez, I. (2022). Output feedback robust control for teleoperated manipulator robots with different workspace. *Expert Systems with Applications*, 206(June), 117838.
<https://doi.org/10.1016/j.eswa.2022.117838>
- Satya Durga Manohar Sahu, V., Samal, P., & Kumar Panigrahi, C. (2022). Modelling, and control techniques of robotic manipulators: A review. *Materials Today: Proceedings*, 56, 2758–2766.
<https://doi.org/10.1016/j.matpr.2021.10.009>
- Xu, J., Xie, Z., Yue, H., Lu, Y., & Yang, F. (2022). A triboelectric multifunctional sensor based on the controlled buckling structure for motion monitoring and bionic tactile of soft robots. *Nano Energy*, 104(PA), 107845.
<https://doi.org/10.1016/j.nanoen.2022.107845>

